A global atlas of substrate specificities for the human serine/threonine kinome

Jared L. Johnson[1,2]*, Tomer M. Yaron[1,2,3,4,5]*, Emily M. Huntsman[1,2], Alexander Kerelsky[1,2,3], Junho Song[1,2], Amit Regev[1,2], Ting-Yu Lin[1,2,6], Katarina Liberatore[1,2], Daniel M. Cizin[1,2], Benjamin M. Cohen[1,2], Neil Vasan[7,8], Yilun Ma[1,2], Konstantin Krismer[9,10], Jaylissa Torres Robles[11,12], Bert van de Kooij[13], Anne E. van Vlimmeren[13], Nicole Andrée-Busch[14], Norbert Käufer[14], Maxim V. Dorovkov[15], Alexey G. Ryazanov[15], Yuichiro Takagi[16], Edward R. Kastenhuber[1,2], Marcus D. Goncalves[1,17], Olivier Elemento[3,4], Dylan J. Taatjes[18], Alexandre Maucuer[19], Akio Yamashita[20], Alexei Degterev[21], Rune Linding[22], John Blenis[1,23,24], Peter V. Hornbeck[25], Benjamin E. Turk[11]§, Michael B. Yaffe[10,26]§, Lewis C. Cantley[1,2]§

Corresponding authors:

Lewis C. Cantley, Ph.D.

Meyer Director, Sandra and Edward Meyer Cancer Center
Professor of Cancer Biology in Medicine
Weill Cornell Medicine
Tel: ++1 (646) 962-632
Fax: ++1 (646) 962-0575
Email: LCantley@med.cornell.edu,

Michael B. Yaffe, M.D., Ph.D.

Director, MIT Center for Precision Cancer Medicine
Professor of Biology and Biological Engineering Koch Institute for Integrative Cancer Research
Senior Associate Member, Broad Institute
Massachusetts Institute of Technology
Phone: ++1 (617) 452-2103
Lab Suite: ++1 (617) 452-2442
Fax: ++1 (617) 452-4978
Email: myaffe@mit.edu

Benjamin E. Turk, Ph.D.

Associate Professor of Pharmacology
Director of Medical Studies, Pharmacology
Yale School of Medicine
Office: ++1 (203) 737-2494
Fax: ++1 (203) 785-7670
Lab: ++1 (203) 785-3259
Email: ben.turk@yale.edu

[1]Meyer Cancer Center, Weill Cornell Medicine, New York, NY, USA.
[2]Department of Medicine, Weill Cornell Medicine, New York, NY, USA.
[3]Englander Institute for Precision Medicine, Institute for Computational Biomedicine, Weill Cornell Medicine, New York, NY, USA.
[4]Department of Physiology and Biophysics, Weill Cornell Medicine, New York, NY, USA.
[5]Tri-Institutional PhD Program in Computational Biology & Medicine, Weill Cornell Medicine/Memorial Sloan Kettering Cancer Center/The Rockefeller University, New York, NY, USA.
[6]Weill Cornell Graduate School of Medical Sciences, Cell and Developmental Biology Program, New York, NY, USA
[7]Department of Medicine, Division of Hematology/Oncology, Columbia University Irving Medical Center, New York, NY, USA.
[8]Herbert Irving Comprehensive Cancer Center, Columbia University Irving Medical Center, New York, NY, USA
[9]Computer Science and Artificial Intelligence Laboratory, Massachusetts Institute of Technology, Cambridge, MA, USA
[10]Center for Precision Cancer Medicine, Koch Institute for Integrative Cancer Biology, Departments of Biology and Biological Engineering, Massachusetts Institute of Technology, Cambridge, MA 02142, USA
[11]Department of Pharmacology, Yale School of Medicine, New Haven, CT, USA.
[12]Department of Chemistry, Yale University, New Haven, CT, USA
[13]Center for Precision Cancer Medicine, Koch Institute for Integrative Cancer Biology, Departments of Biology and Biological Engineering, Massachusetts Institute of Technology, Cambridge, MA, USA
[14]Institute of Genetics, Technische Universität Braunschweig, 38106 Braunschweig, Germany.
[15]Department of Pharmacology, Rutgers Robert Wood Johnson Medical School, Piscataway, NJ, USA.
[16]Department of Biochemistry and Molecular Biology, Indiana University School of Medicine, Indianapolis, IN, USA.
[17]Division of Endocrinology, Weill Cornell Medicine, New York, NY, USA.
[18]Department of Biochemistry, University of Colorado, Boulder, CO, USA.
[19]SABNP, Univ Evry, INSERM U1204, Université Paris-Saclay, 91025 Evry, France.
[20]Department of Investigative Medicine, graduate school of medicine, University of the Ryukyus, 207 Uehara, Nishihara-cho, Okinawa, Japan.
[21]Department of Developmental, Molecular and Chemical Biology, Tufts University School of Medicine, Boston, MA, USA.
[22]Rewire Tx, Humboldt-Universität zu Berlin, Invalidenstr. 42, 10115, Berlin, Germany
[23]Department of Pharmacology, Weill Cornell Medicine, New York, NY, USA.
[24]Department of Biochemistry, Weill Cornell Medicine, New York, NY, USA.
[25]Department Of Bioinformatics, Cell Signaling Technology, Danvers, MA, USA.
[26]Divisions of Acute Care Surgery, Trauma, and Surgical Critical Care, and Surgical Oncology, Department of Surgery, Beth Israel Deaconess Medical Center, Harvard Medical School, Boston MA 02215
*These authors contributed equally to this study.

ABSTRACT

Protein phosphorylation is one of the most widespread post-translational modifications in biology. With the advent of mass spectrometry-based phosphoproteomics, more than 200,000 sites of serine and threonine phosphorylation have been reported, of which several thousand have been associated with human diseases and biological processes. For the vast majority of phosphorylation events, it is not yet known which of the more than 300 protein Ser/Thr kinases encoded in the human genome is responsible. Here, we utilize synthetic peptide libraries to profile the substrate sequence specificity of nearly every functional human Ser/Thr kinase. Viewed in its entirety, the substrate specificity of the kinome was substantially more diverse than expected and was driven extensively by negative selectivity. Our kinome-wide dataset was used to computationally annotate and identify the most likely protein kinases for every reported phosphorylation site in the human Ser/Thr phosphoproteome. For the small minority of phosphosites where the protein kinases involved have been previously identified, our predictions were in excellent agreement. When this approach was applied to examine the signaling response of tissues and cell lines to hormones, growth factors, targeted inhibitors, and environmental or genetic perturbations, it revealed unexpected insights into pathway complexity and compensation. Overall, these studies reveal the full extent of substrate specificity of the human Ser/Thr kinome, illuminate cellular signaling responses, and provide a rich resource to link unannotated phosphorylation events to biological pathways.

INTRODUCTION

Phosphorylation of proteins on serine, threonine, tyrosine, and histidine residues controls nearly every aspect of eukaryotic cellular function[1-4]. Misregulation of protein kinase signaling commonly results in human disease[5-8]. Deciphering the cellular roles of any protein kinase requires elucidation of its downstream effector substrates. The majority of kinase-substrate relationships that have been published to date, however, involve a relatively small number of well-studied protein kinases, while few, if any, substrates have been identified for the majority of the ~300 human protein Ser/Thr kinases within the human kinome[9-11]. This lack of knowledge of kinase-substrate relationships limits the interpretation of large mass spectrometry-based

116 phosphoproteomic datasets, which to date have collectively reported over 200,000 Ser and Thr
117 phosphorylation sites on human proteins[12-15]. The specific kinases responsible for these
118 phosphorylation events have been reported for <4% of these sites[15], severely limiting the
119 understanding of cellular phosphorylation networks.

120 Well-studied serine/threonine kinases are generally known to recognize specific amino
121 acid residues at multiple positions surrounding the site of phosphorylation[16-21]. This short linear
122 motif, which is characteristic of a given protein kinase, ensures fidelity in signaling pathways
123 regulating phosphorylation at a given Ser or Thr residue. Knowledge of kinase recognition motifs
124 can facilitate discovery of new substrates, for example by scanning phosphoproteomics data for
125 matching sequences. However, to date, phosphorylation site sequence motifs are known for only
126 a subset of the human protein Ser/Thr kinome. In some cases, kinase recognition motifs have been
127 inferred by alignment of known cellular phosphorylation sites that have been experimentally
128 identified over many years. This process is slow and laborious and limited to kinases with large
129 numbers of established substrates. We have previously described combinatorial peptide library
130 screening methods that allow for rapid determination of specificity for individual kinases based on
131 phosphorylation of peptide substrates[22,23]. Here, we apply those methods to experimentally
132 determine the optimal substrate specificity for nearly the entire human serine-threonine kinome,
133 characterize the relationship between kinases based on their motifs, and computationally utilize
134 this data to identify the most likely protein kinase to phosphorylate any site identified by mass
135 spectrometry or other techniques. Finally, we show how this information can be applied to capture
136 complex changes in signaling pathways in cells and tissues following genetic, pharmacological,
137 metabolic, and environmental perturbations.
138
139 **RESULTS**
140
141 **Phosphorylation site substrate specificity of the human serine-threonine kinome**
142
143 Substrate recognition motifs across the human Ser-Thr kinome were determined by
144 performing positional scanning peptide array (PSPA) analysis. We used a previously reported
145 combinatorial peptide library that systematically substitutes each of 22 amino acids (20 natural
146 amino acids plus phospho-Thr and phospho-Tyr) at nine positions surrounding a central phospho-

147 acceptor position containing equivalent amounts of Ser and Thr (Fig. 1a)[23]. Using purified
148 recombinant kinase preparations, we successfully obtained phosphorylation site motifs for 303
149 Ser/Thr kinases, covering every branch of the human Ser/Thr kinase family tree as well as a
150 collection of atypical protein kinases (Fig. 1b, Fig. S1). The large majority of these kinases,
151 including 86 understudied "dark" kinases, had not been previously profiled.

152 Position-specific scoring matrices (PSSMs) derived from quantified PSPA data were
153 analyzed by hierarchical clustering to compare kinase substrate motifs across the kinome (Fig. 2).
154 As expected, kinases sharing substantial sequence identity displayed a high degree of similarity in
155 their optimal substrate motifs. However, we found many cases where clustering by PSSM did not
156 strictly recapitulate evolutionary phylogenetic relationships between kinases inferred from their
157 primary sequences (Fig. 2). Instead, members of most major kinase groups were distributed
158 throughout the dendrogram, reflecting numerous examples where kinases with low overall
159 sequence identity have converged to phosphorylate similar optimal sequence motifs. For example,
160 we found that a number of distantly related kinases (in the YANK, casein kinase 1 and 2, GRK,
161 and TGF-β receptor families) converged to phosphorylate similar sequence motifs despite their
162 very disparate locations on the kinome tree (Fig. 2, Cluster 3).

163 Overall inspection of sequence motifs associated with various branches of the motif-based
164 dendrogram revealed that approximately ~60% of the Ser-Thr kinome could be represented by
165 simple assignment to one of three previously observed motif classes: selectivity for basic residues
166 N-terminal to the phosphorylation site (Cluster 1, Fig. 2), directed by a proline residue at the +1
167 position (Cluster 2), or a general preference for negatively charged (acidic and phosphorylated)
168 residues at multiple positions (Cluster 3)[17,20,24,25]. Notably, more than half of all reported
169 phosphorylation sites observed by MS could be assigned to one of these three signatures (Fig. S2).
170 However, each of these motif classes could be further subcategorized based on selectivity both for
171 and against distinct sets of residues at other positions, reflecting considerable diversity within these
172 clusters (Figs. S3, S4, and S5).

173 The remaining ~40% of the Ser/Thr kinome comprised many smaller groups that displayed
174 unique sequence determinants (Fig. 2, Clusters 4 – 17). For example, motifs for the DNA-damage
175 response kinases (ATM, ATR, DNAPK and SMG1) clustered into a group that primarily selected
176 a Gln residue at the +1 position (Cluster 5), consistent with previous studies[26,27]. Notably, several
177 clusters displayed shared consensus motifs that have not been well recognized previously, such as

178 the group including the IRAK, IRE, WNK, SNRK, and RIP kinases (Cluster 13), whose substrate
179 motifs contained basic residues both N- and C-terminal to the phosphorylation site with dominant
180 selection for aromatic residues in the +3 position. As another example, the kinases LKB1,
181 CAMKK, PINK1, and PBK (Cluster 14) primarily recognized hydrophobic residues N-terminal to
182 the phosphorylation site in combination with selection for turn-promoting residues (Gly or Asn)
183 in the +1 position. Structural modeling of kinase-peptide complexes revealed complementary
184 features within the kinase catalytic clefts likely responsible for recognition of these motifs (Fig.
185 S6a,b).

186 An important and less generally recognized feature that dominated the clustering was
187 strong negative selection against either positively or negatively charged residues at distinct
188 positions within a motif, suggesting that electrostatic filtering strongly influences kinase substrate
189 selection throughout the kinome[28,29]. We identified additional classes of amino acids, such as
190 hydrophobic residues, that are selected against by a variety of kinases. These trends suggest that
191 substrate avoidance plays a fundamental role in dictating correct kinase-substrate interactions[30,31].

192 Unexpectedly, we observed that many kinases (129 out of 303) selected either a phospho-
193 Thr or a phospho-Tyr as the preferred amino acid in at least one position within the motif (Fig.
194 S1). In addition to kinases whose dependence on phospho-priming was previously known [GSK3,
195 casein kinase 1, and casein kinase 2 families[32,33], Cluster 3], this phenomenon was particularly
196 evident for the GRK and YANK family kinases (Fig. S5), both of which have complementary
197 basic residues within their catalytic domains (Fig. S6c,d). Intriguingly, individual GRK family
198 members showed unique and specific selection for the location of the phospho-Thr or phospho-
199 Tyr residue within their substrate peptides. GRKs are best known for their role in desensitization
200 of G-protein coupled receptors (GPCRs), where multisite phosphorylation induces binding of
201 arrestin proteins to inhibit signaling[34,35]. Our findings suggest that the capacity for only seven
202 GRKs to differentially regulate 800 distinct GPCRs likely involves a complex interplay between
203 initial sequence-specific phosphopriming of GPCRs by other serine/threonine and tyrosine
204 kinases, followed by a second level of specificity resulting from GRK-dependent phosphorylation
205 and subsequent recognition by a small number of β-arrestins.

206 Features of substrate recognition motifs across the entire kinome could be structurally
207 rationalized based on the presence of specificity-determining residues at particular positions within
208 the kinase catalytic domain[36,37], leading to both expected and unexpected discoveries. For example,

209 we found half of the kinases to display some degree of selectivity for either a Ser or a Thr as the
210 phospho-acceptor residue (Fig. S7). Consistent with our previously published observations[38], Ser
211 or Thr phospho-acceptor site preference strongly correlated with the identity of the 'DFG+1'
212 residue within the kinase activation loop, with bulky residues (Phe, Trp, Tyr) at this position in
213 Ser-selective protein kinases and β-branched residues (Val, Ile, Thr) at this position in Thr-
214 selective kinases. For some DFG+1 residues, however, Ser vs. Thr selectivity was unexpectedly
215 context dependent. For instance, a Leu residue in the DFG+1 position was observed in both Ser-
216 selective and dual specificity kinases, while a DFG+1 Ala residue resulted in a preference for Thr
217 phosphorylation in the context of some kinases (e.g., the mitogen-activated protein kinase kinase
218 kinases [MAP3Ks]), but a preference for Ser specificity in others (the IκB kinases [IKKs]). These
219 observations, notable only within the context of the complete Ser/Thr kinome, indicate that
220 additional residues beyond the previously established DFG+1 position can influence Ser/Thr
221 specificity in a context-dependent manner.
222
223 **Phosphorylation motifs for the entire human serine/threonine kinome allow comprehensive**
224 **annotation of the human phosphoproteome**
225
226 Comprehensive knowledge of the human Ser/Thr kinase specificity has the potential to 'de-
227 orphanize' the large number of reported phosphorylation sites with no associated kinase. To do so
228 we generated a kinome-wide annotation of the human Ser/Thr phosphoproteome by
229 computationally ranking each of ~50,000 high confidence phosphorylation sites against each
230 Ser/Thr kinase motif (Fig. 3a, Table S2)[39]. Interestingly, more than 98% of these phosphorylation
231 sites ranked favorably for at least one kinase we profiled (i.e., the site scored in the top 10% of all
232 sites in the human phosphoproteome for that kinase). These annotations were strongly concordant
233 with sites for which protein kinases involved have been previously identified. For phosphorylation
234 sites whose upstream kinase has been previously verified by at least 3 independent reports,
235 encompassing 969 sites and over 1/3rd of the kinome, our motif-based approach yielded a median
236 percentile of 93% (i.e., the reported site received a higher score than 93% of all putative
237 phosphorylation sites in the phosphoproteome for its established kinase) (Fig. S8a). Furthermore,
238 when we back-mapped the motifs of all 303 profiled kinases onto the literature-reported
239 phosphorylation sites, our approach yielded a median reported kinase percentile of 92%, (i.e., the

240 reported kinase scored more favorably than 92% of all profiled kinases in our atlas for its
241 established substrate) (Fig. S8b). These rankings further improved when we considered kinase-
242 substrate pairs with higher numbers of prior reports (Figs. S9, S10), suggesting that in a large
243 majority of cases the linear sequence context of phosphorylation sites contributes substantially to
244 kinase-substrate relationships.

245 Remarkably, motif predictions alone successfully identified numerous prominently studied
246 kinase substrate relationships. For example, phosphorylase kinases PHKG1 and PHKG2 emerged
247 as the top two hits (out of 303 kinases) for phosphorylating Ser15 of glycogen phosphorylase (Fig.
248 3b). This phosphoregulatory event, the very first to be discovered[40,41], opened up the entire field
249 of phosphorylation-dependent signal transduction. The most highly cited kinase-substrate
250 interaction reported to date is phosphorylation of the tumor suppressor p53 at Ser15 by the DNA
251 damage-activated kinase ATM, which scored as the top-ranking kinase associated with that site
252 (Fig. 3c). Notably, other kinases reported to phosphorylate the same site, ATR, SMG1, and
253 DNAPK, scored within the top 4 predicted kinases[42,43].

254 Our approach could also correctly identify kinases for phosphorylation events driven by
255 substrate co-localization or non-catalytic docking interactions, where we expected less dependence
256 on the phosphorylation site motifs of their kinases. For example, we correctly identified both the
257 mitochondrial-localized phosphorylation of pyruvate dehydrogenase by the pyruvate
258 dehydrogenase kinases (Fig. S11a) and the docking-driven phosphorylation of the MAP kinase
259 ERK by MEK (Fig. S11b)[44-48]. Interestingly, the phosphorylation site on ERK was selected *against*
260 by nearly every human protein kinase we profiled except MEK, explaining how ERK can be
261 exclusively regulated by MEK while avoiding phosphorylation by the kinome at large. Finally,
262 our approach could tease apart kinase subfamilies with similar motifs and correctly assign them to
263 their established substrates. For example, we could distinguish the CDK family kinases assuming
264 classical roles in cell cycle progression (CDK1,2,3,4 and 6) from the subset of CDKs that govern
265 gene transcription (CDK7,8,9,12,13 and 19) (Fig. S12)[49,50].

266 Functional annotation of the human phosphoproteome allowed us to explore global trends
267 in kinase-substrate interactions. We found that most phosphorylation sites could be assigned to a
268 very small number of putative kinases (i.e., BRAF-MEK1, ATM-p53, and CDK4-Rb in Fig. 3d).
269 However, a substantial minority of sites lacked unique negative sequence-discriminating features,
270 and instead matched well to the optimal phosphorylation motifs for a greater number of kinases

271 (i.e., Ser119 of CREB, Ser9 of GSK3B, and Thr1079 of LATS1; Fig. 3d) [25,51-53]. This could suggest
272 the importance of other kinase-determining factors (scaffolds, localization, etc.) for proper kinase-
273 substrate recognition, or may indicate that these specific phosphorylation sites are points of
274 convergence for multiple signaling pathways. For example, cAMP response element binding
275 protein (CREB) is canonically phosphorylated at Ser119 by cAMP-dependent protein kinase
276 (PKA), however, numerous prior reports demonstrate that a broad range of cellular stimuli and
277 drug perturbations impinge on phosphorylation of this site by no less than ten distinct kinases[15,54].
278 Taken together, these findings suggest that the presence of negative selectivity elements flanking
279 a putative phosphorylation site can be used to insulate a substrate from inappropriate
280 phosphorylation by dozens of related kinases, while the absence of such negative selectivity can
281 allow protein kinases in distinct pathways to converge on the same target.
282
283 **Global motif analysis reveals how kinase perturbations and pathway rewiring reshape the**
284 **phosphoproteome**
285
286 Cell signaling networks are complex and dynamic. Perturbation of kinase signaling
287 pathways by genetic manipulations, treatment with growth factors and ligands, environmental
288 stress, or small molecule inhibitors reshapes the phosphoproteome through both direct and indirect
289 effects as a consequence of secondary signaling responses and/or off-target effects from the
290 experimental treatment[13,55,56]. Due to the interconnected and dynamic nature of phosphorylation
291 networks, distinguishing initial signaling events from those that result from the subsequent
292 activation of additional signaling pathways is a common and challenging problem. We reasoned
293 that kinases underlying both primary and secondary phosphorylation events could potentially be
294 revealed by a global motif-based analysis of changes in the corresponding phosphoproteome. To
295 test this idea, we used publicly available MS datasets from cells collected in the absence or
296 presence of various perturbations and scored all phosphorylation sites with our atlas of
297 serine/threonine kinase motifs. Kinase motifs significantly enriched or depleted following
298 experimental treatment were then represented as volcano plots of motif frequencies and adjusted
299 p-values (Fig. 4a).
300 Using this approach, we found that sequence motifs corresponding to the most direct target
301 of a genetic or chemical perturbation were among the most significantly regulated (seen, for

302 example, with genetic deletion of the secreted primordial casein kinase FAM20C (Fig. 4b))[57].
303 When quantitative phosphoproteomics data from HepG2 cells lacking FAM20C[58] were analyzed
304 by our kinome-wide dataset, the most downregulated kinase recognition motif corresponded to
305 that of FAM20C. Similarly, when skeletal muscle-like myotube cells were stimulated for 30
306 minutes with isoproterenol[59], the most upregulated phosphorylation motifs corresponded to
307 multiple isoforms of cAMP-dependent protein kinase (PKA), canonical effector kinases
308 downstream of the β_1 and β_2 adrenergic receptors (Fig. 4c)[60,61]. Of note, PKA motifs are highly
309 similar to those of several other basophilic kinases yet we could identify their enrichment in this
310 scenario. In addition, our comprehensive serine/threonine kinome motif collection elucidated
311 secondary signaling events in a dataset from HeLa cells arrested in mitosis using the PLK1
312 inhibitor BI-2536 (Fig. 4d)[62] where, in addition to observing a striking downregulation of
313 substrates containing the optimal PLK1 motif, we also noted significant upregulation of substrates
314 phosphorylated by ATM and ATR. This finding is in good agreement with prior reports that PLK1
315 can suppress DNA damage signaling in mitotic cells[63,64].
316 Our motif-based analysis could also be used to reveal key signaling events resulting from
317 more complex interventions. For example, we interrogated phosphoproteomic data from A549
318 cells treated with 6 Gy of ionizing radiation (Fig. 4e)[65]. Our analysis revealed the up- and down-
319 regulation of numerous signaling pathways, including upregulation of canonical kinases involved
320 in the DNA damage response (ATM, ATR, DNAPK, SMG1) and downregulation of canonical
321 kinases involved in cell cycle progression (CDK1, 2, 4, and 6) consistent with G1/S and G2/M
322 arrest. Furthermore, we found up- and down-regulation of less appreciated DNA damage-
323 responsive kinases [MAPKAPK2 [66,67], PLK3 [68], and LRKK2 [69]].
324 The full collection of serine/threonine kinome motifs also allowed temporal dynamics of
325 signaling to be resolved from time-resolved phosphoproteomic datasets. For example, motif-based
326 analysis of phosphoproteomic data from insulin-treated 3T3-L1 adipocytes[70] revealed rapid
327 activation of the phosphoinositide 3-kinase signaling pathway within 1 minute after insulin
328 stimulation followed by subsequent activation of the MAPK pathway, together with
329 downregulation of AMP- and cAMP-dependent protein kinases within 60 minutes (Fig. 4f).
330 Similarly, phosphoproteomic data analysis from LPS-stimulated dendritic cells[71] suggested
331 marked upregulation at 30 minutes of a set of stress-activated kinases including the IKKs, JNK
332 and p38 MAPKs, along with the MAPKAPK family of p38 effector kinases, followed within 4

333 hours by subsequent upregulation of the PIM kinases and suppression of the MAPKs in parallel
334 with the downregulation of their upstream MAPK3Ks (MEKK1, MEKK2, and ZAK)[72,73],
335 suggestive of a negative feedback loop (Fig. 4g). Thus, comprehensive motif-based approaches,
336 when applied to time-resolved phosphoproteomics experiments, can decipher the distinct temporal
337 dynamics of different groups of kinases.
338
339 **DISCUSSION**
340
341 This work presents the full spectrum of substrate motifs of the human serine/threonine
342 kinome and provides an unbiased global framework to further explore their cellular functions.
343 Globally, these motifs are substantially more diverse than expected, suggesting a broader substrate
344 repertoire of the kinome. Hierarchical clustering of this dataset reorganized the kinome into 17
345 motif-classes and introduced several novel shared motif features (Fig. 2). For kinases with similar
346 motifs, we saw multiple cases where their minor differences translated into dramatically different
347 substrate predictions and motif enrichments (Fig. S11, Fig. 4c-g) and rationalized how such
348 biochemically similar kinases can have divergent biological roles.
349 The serine/threonine kinases we profiled were, almost without exception, strongly
350 discriminatory against specific motif features. This negative selection rationalizes how kinases
351 sharing similar positively selected residues in their motifs can regulate distinct signaling pathways
352 with specialized cellular functions, and how substrates are insulated from inappropriate
353 phosphorylation by irrelevant kinases. Intriguingly, these findings suggest that fidelity in kinase
354 signaling pathways is largely achieved through selective pressure on substrates to avoid
355 phosphorylation by the majority of irrelevant kinases, and that this may occur by tuning the amino
356 acid sequences surrounding the phosphorylation sites to be disfavored by non-cognate kinases.
357 Since this negative selection contributes substantially to proper substrate recognition, accurate
358 identification of kinase-substrate relationships requires a comprehensive knowledge of kinase
359 phosphorylation motifs – not only for an individual kinase of interest, but also for all other kinases
360 in the human kinome that might compete for the same substrate pool.
361 When this kinome-wide dataset was used to predict specific kinases responsible for
362 substrate phosphorylation solely based on the amino acid sequence surrounding the
363 phosphorylation site, the results were remarkably accurate at identifying correct kinase-substrate

relationships, even without knowledge of tissue specificity, scaffolding effects, or subcellular localization. Including such additional information is likely to further improve these predictive approaches[74,75]. Interrogation of MS phosphoproteomic datasets using this global collection of motifs yielded new potential biological insights and new putative kinase substrates (Fig. 4). For example, in cells undergoing exposure to ionizing radiation (Fig. 4e), ATM was predicted to target 35 of the phosphorylation sites that were upregulated, most of which have never been associated as substrates for ATM (Table S3). As the application of phosphoproteomics to human clinical samples and disease model systems continues to advance[76], our comprehensive motif-based approach will be uniquely equipped to unravel complex signaling events that underlie human disease progressions, mechanisms of cancer drug resistance, dietary interventions, and other important physiological processes. In sum, we foresee this providing a valuable resource for a broad spectrum of researchers who study signaling pathways in human biology and disease.

REFERENCES

1 Cohen, P. The origins of protein phosphorylation. *Nature cell biology* **4**, E127-E130 (2002).

2 Manning, G., Whyte, D. B., Martinez, R., Hunter, T. & Sudarsanam, S. The protein kinase complement of the human genome. *Science* **298**, 1912-1934 (2002).

3 Fuhs, S. R. & Hunter, T. pHisphorylation: the emergence of histidine phosphorylation as a reversible regulatory modification. *Current opinion in cell biology* **45**, 8-16 (2017).

4 Hunter, T. Why nature chose phosphate to modify proteins. *Philosophical Transactions of the Royal Society B: Biological Sciences* **367**, 2513-2516 (2012).

5 Blume-Jensen, P. & Hunter, T. Oncogenic kinase signalling. *Nature* **411**, 355-365 (2001).

6 Lahiry, P., Torkamani, A., Schork, N. J. & Hegele, R. A. Kinase mutations in human disease: interpreting genotype–phenotype relationships. *Nature Reviews Genetics* **11**, 60-74 (2010).

7 Ferguson, F. M. & Gray, N. S. Kinase inhibitors: the road ahead. *Nature reviews Drug discovery* **17**, 353-377 (2018).

8 Wu, P., Nielsen, T. E. & Clausen, M. H. Small-molecule kinase inhibitors: an analysis of FDA-approved drugs. *Drug discovery today* **21**, 5-10 (2016).

9 Berginski, M. E. *et al.* The Dark Kinase Knowledgebase: an online compendium of knowledge and experimental results of understudied kinases. *Nucleic acids research* **49**, D529-D535 (2021).

10 Moret, N. *et al.* A resource for exploring the understudied human kinome for research and therapeutic opportunities. *BioRxiv*, 2020.2004. 2002.022277 (2021).

11 Needham, E. J., Parker, B. L., Burykin, T., James, D. E. & Humphrey, S. J. Illuminating the dark phosphoproteome. *Science signaling* **12**, eaau8645 (2019).

402 12 Lemeer, S. & Heck, A. J. The phosphoproteomics data explosion. *Current opinion in*
403 *chemical biology* **13**, 414-420 (2009).
404 13 Aebersold, R. & Mann, M. Mass-spectrometric exploration of proteome structure and
405 function. *Nature* **537**, 347-355 (2016).
406 14 Riley, N. M. & Coon, J. J. Phosphoproteomics in the age of rapid and deep proteome
407 profiling. *Analytical chemistry* **88**, 74-94 (2016).
408 15 Hornbeck, P. V. *et al.* 15 years of PhosphoSitePlus®: integrating post-translationally
409 modified sites, disease variants and isoforms. *Nucleic Acids Research* **47**, D433-D441
410 (2019).
411 16 Kemp, B. E., Graves, D. J., Benjamini, E. & Krebs, E. G. Role of multiple basic residues in
412 determining the substrate specificity of cyclic AMP-dependent protein kinase. *Journal of*
413 *Biological Chemistry* **252**, 4888-4894 (1977).
414 17 Kemp, B. E. & Pearson, R. B. Protein kinase recognition sequence motifs. *Trends in*
415 *biochemical sciences* **15**, 342-346 (1990).
416 18 Marin, O., MEGGIO, F., MARCHIORI, F., BORIN, G. & PINNA, L. A. Site specificity of casein
417 kinase-2 (TS) from rat liver cytosol: A study with model peptide substrates. *European*
418 *journal of biochemistry* **160**, 239-244 (1986).
419 19 Clark-Lewis, I., Sanghera, J. S. & Pelech, S. Definition of a consensus sequence for
420 peptide substrate recognition by p44mpk, the meiosis-activated myelin basic protein
421 kinase. *Journal of Biological Chemistry* **266**, 15180-15184 (1991).
422 20 Pinna, L. A. & Ruzzene, M. How do protein kinases recognize their substrates?
423 *Biochimica et Biophysica Acta (BBA)-Molecular Cell Research* **1314**, 191-225 (1996).
424 21 Meggio, F. & Pinna, L. A. One-thousand-and-one substrates of protein kinase CK2? *The*
425 *FASEB Journal* **17**, 349-368 (2003).
426 22 Songyang, Z. *et al.* Use of an oriented peptide library to determine the optimal
427 substrates of protein kinases. *Current biology* **4**, 973-982 (1994).
428 23 Hutti, J. E. *et al.* A rapid method for determining protein kinase phosphorylation
429 specificity. *Nature methods* **1**, 27-29 (2004).
430 24 Mok, J. *et al.* Deciphering protein kinase specificity through large-scale analysis of yeast
431 phosphorylation site motifs. *Science signaling* **3**, ra12-ra12 (2010).
432 25 Pearce, L. R., Komander, D. & Alessi, D. R. The nuts and bolts of AGC protein kinases.
433 *Nature reviews Molecular cell biology* **11**, 9-22 (2010).
434 26 Kim, S.-T., Lim, D.-S., Canman, C. E. & Kastan, M. B. Substrate specificities and
435 identification of putative substrates of ATM kinase family members. *Journal of Biological*
436 *Chemistry* **274**, 37538-37543 (1999).
437 27 O'Neill, T. *et al.* Utilization of oriented peptide libraries to identify substrate motifs
438 selected by ATM. *Journal of Biological Chemistry* **275**, 22719-22727 (2000).
439 28 Shah, N. H. *et al.* An electrostatic selection mechanism controls sequential kinase
440 signaling downstream of the T cell receptor. *Elife* **5**, e20105 (2016).
441 29 Shah, N. H., Löbel, M., Weiss, A. & Kuriyan, J. Fine-tuning of substrate preferences of the
442 Src-family kinase Lck revealed through a high-throughput specificity screen. *Elife* **7**,
443 e35190 (2018).

30 Zhu, G. *et al.* Exceptional disfavor for proline at the P+ 1 position among AGC and CAMK kinases establishes reciprocal specificity between them and the proline-directed kinases. *Journal of Biological Chemistry* **280**, 10743-10748 (2005).
31 Alexander, J. *et al.* Spatial exclusivity combined with positive and negative selection of phosphorylation motifs is the basis for context-dependent mitotic signaling. *Science signaling* **4**, ra42-ra42 (2011).
32 Fiol, C. J., Wang, A., Roeske, R. W. & Roach, P. J. Ordered multisite protein phosphorylation. Analysis of glycogen synthase kinase 3 action using model peptide substrates. *Journal of Biological Chemistry* **265**, 6061-6065 (1990).
33 Flotow, H. *et al.* Phosphate groups as substrate determinants for casein kinase I action. *Journal of Biological Chemistry* **265**, 14264-14269 (1990).
34 Reiter, E. & Lefkowitz, R. J. GRKs and β-arrestins: roles in receptor silencing, trafficking and signaling. *Trends in endocrinology & metabolism* **17**, 159-165 (2006).
35 Moore, C. A., Milano, S. K. & Benovic, J. L. Regulation of receptor trafficking by GRKs and arrestins. *Annu. Rev. Physiol.* **69**, 451-482 (2007).
36 Bradley, D. *et al.* Sequence and Structure-Based Analysis of Specificity Determinants in Eukaryotic Protein Kinases. *Cell reports* **34**, 108602 (2021).
37 Taylor, S. S. & Kornev, A. P. Protein kinases: evolution of dynamic regulatory proteins. *Trends in biochemical sciences* **36**, 65-77 (2011).
38 Chen, C. *et al.* Identification of a major determinant for serine-threonine kinase phosphoacceptor specificity. *Molecular cell* **53**, 140-147 (2014).
39 Obenauer, J. C., Cantley, L. C. & Yaffe, M. B. Scansite 2.0: Proteome-wide prediction of cell signaling interactions using short sequence motifs. *Nucleic acids research* **31**, 3635-3641 (2003).
40 Fischer, E. H., Graves, D. J., Crittenden, E. R. S. & Krebs, E. G. Structure of the site phosphorylated in the phosphorylase b to a reaction. *Journal of Biological Chemistry* **234**, 1698-1704 (1959).
41 Wolf, D. P., Fischer, E. H. & Krebs, E. G. Amino acid sequence of the phosphorylated site in rabbit liver glycogen phosphorylase. *Biochemistry* **9**, 1923-1929 (1970).
42 Lakin, N. D. & Jackson, S. P. Regulation of p53 in response to DNA damage. *Oncogene* **18**, 7644-7655 (1999).
43 Gehen, S. C., Staversky, R. J., Bambara, R. A., Keng, P. C. & O'Reilly, M. A. hSMG-1 and ATM sequentially and independently regulate the G1 checkpoint during oxidative stress. *Oncogene* **27**, 4065-4074 (2008).
44 Linn, T. C., Pettit, F. H. & Reed, L. J. α-Keto acid dehydrogenase complexes, X. Regulation of the activity of the pyruvate dehydrogenase complex from beef kidney mitochondria by phosphorylation and dephosphorylation. *Proceedings of the National Academy of Sciences* **62**, 234-241 (1969).
45 Kholodenko, B. N., Hancock, J. F. & Kolch, W. Signalling ballet in space and time. *Nature reviews Molecular cell biology* **11**, 414-426 (2010).
46 Ubersax, J. A. & Ferrell Jr, J. E. Mechanisms of specificity in protein phosphorylation. *Nature reviews Molecular cell biology* **8**, 530-541 (2007).
47 Endicott, J. A., Noble, M. E. & Johnson, L. N. The structural basis for control of eukaryotic protein kinases. *Annual review of biochemistry* **81**, 587-613 (2012).

488 48 Xu, B.-e., Wilsbacher, J. L., Collisson, T. & Cobb, M. H. The N-terminal ERK-binding site of
489 MEK1 is required for efficient feedback phosphorylation by ERK2 in vitro and ERK
490 activation in vivo. *Journal of Biological Chemistry* **274**, 34029-34035 (1999).
491 49 Malumbres, M. *et al.* Cyclin-dependent kinases: a family portrait. *Nature cell biology* **11**,
492 1275-1276 (2009).
493 50 Eick, D. & Geyer, M. The RNA polymerase II carboxy-terminal domain (CTD) code.
494 *Chemical reviews* **113**, 8456-8490 (2013).
495 51 Cohen, P. & Frame, S. The renaissance of GSK3. *Nature reviews Molecular cell biology* **2**,
496 769-776 (2001).
497 52 Meng, Z. *et al.* MAP4K family kinases act in parallel to MST1/2 to activate LATS1/2 in the
498 Hippo pathway. *Nature communications* **6**, 1-13 (2015).
499 53 Doble, B. W. & Woodgett, J. R. GSK-3: tricks of the trade for a multi-tasking kinase.
500 *Journal of cell science* **116**, 1175-1186 (2003).
501 54 Johannessen, M., Delghandi, M. P. & Moens, U. What turns CREB on? *Cellular signalling*
502 **16**, 1211-1227 (2004).
503 55 Cravatt, B. F., Simon, G. M. & Yates Iii, J. R. The biological impact of mass-spectrometry-
504 based proteomics. *Nature* **450**, 991-1000 (2007).
505 56 Rigbolt, K. T. & Blagoev, B. in *Seminars in cell & developmental biology.* 863-871
506 (Elsevier).
507 57 Tagliabracci, V. S., Pinna, L. A. & Dixon, J. E. Secreted protein kinases. *Trends in*
508 *biochemical sciences* **38**, 121-130 (2013).
509 58 Tagliabracci, V. S. *et al.* A single kinase generates the majority of the secreted
510 phosphoproteome. *Cell* **161**, 1619-1632 (2015).
511 59 Needham, E. J. *et al.* Phosphoproteomics of acute cell stressors targeting exercise
512 signaling networks reveal drug interactions regulating protein secretion. *Cell reports* **29**,
513 1524-1538. e1526 (2019).
514 60 Walsh, D., Perkins, J. P. & Krebs, E. G. An adenosine 3’, 5’-monophosphate-dependant
515 protein kinase from rabbit skeletal muscle. *Journal of Biological Chemistry* **243**, 3763-
516 3765 (1968).
517 61 Sutherland, E. W. & Rall, T. The relation of adenosine-3', 5'-phosphate and
518 phosphorylase to the actions of catecholamines and other hormones. *Pharmacological*
519 *Reviews* **12**, 265-299 (1960).
520 62 Kettenbach, A. N. *et al.* Quantitative phosphoproteomics identifies substrates and
521 functional modules of Aurora and Polo-like kinase activities in mitotic cells. *Science*
522 *signaling* **4**, rs5-rs5 (2011).
523 63 van Vugt, M. A. *et al.* A mitotic phosphorylation feedback network connects Cdk1, Plk1,
524 53BP1, and Chk2 to inactivate the G2/M DNA damage checkpoint. *PLoS biology* **8**,
525 e1000287 (2010).
526 64 Macůrek, L. *et al.* Polo-like kinase-1 is activated by aurora A to promote checkpoint
527 recovery. *Nature* **455**, 119-123 (2008).
528 65 Winter, M. *et al.* Deciphering the acute cellular phosphoproteome response to
529 irradiation with X-rays, protons and carbon ions. *Molecular & Cellular Proteomics* **16**,
530 855-872 (2017).

531 66 Reinhardt, H. C., Aslanian, A. S., Lees, J. A. & Yaffe, M. B. p53-deficient cells rely on ATM-
532 and ATR-mediated checkpoint signaling through the p38MAPK/MK2 pathway for
533 survival after DNA damage. *Cancer cell* **11**, 175-189 (2007).
534 67 Reinhardt, H. C. & Yaffe, M. B. Kinases that control the cell cycle in response to DNA
535 damage: Chk1, Chk2, and MK2. *Current opinion in cell biology* **21**, 245-255 (2009).
536 68 Xie, S. *et al.* Plk3 functionally links DNA damage to cell cycle arrest and apoptosis at least
537 in part via the p53 pathway. *Journal of Biological Chemistry* **276**, 43305-43312 (2001).
538 69 Gonzalez-Hunt, C. *et al.* Mitochondrial DNA damage as a potential biomarker of LRRK2
539 kinase activity in LRRK2 Parkinson's disease. *Scientific reports* **10**, 1-12 (2020).
540 70 Humphrey, S. J. *et al.* Dynamic adipocyte phosphoproteome reveals that Akt directly
541 regulates mTORC2. *Cell metabolism* **17**, 1009-1020 (2013).
542 71 Mertins, P. *et al.* An integrative framework reveals signaling-to-transcription events in
543 toll-like receptor signaling. *Cell reports* **19**, 2853-2866 (2017).
544 72 Johnson, G. L. & Lapadat, R. Mitogen-activated protein kinase pathways mediated by
545 ERK, JNK, and p38 protein kinases. *Science* **298**, 1911-1912 (2002).
546 73 Gallo, K. A. & Johnson, G. L. Mixed-lineage kinase control of JNK and p38 MAPK
547 pathways. *Nature reviews Molecular cell biology* **3**, 663-672 (2002).
548 74 Miller, C. J. & Turk, B. E. Homing in: mechanisms of substrate targeting by protein
549 kinases. *Trends in biochemical sciences* **43**, 380-394 (2018).
550 75 Linding, R. *et al.* Systematic discovery of in vivo phosphorylation networks. *Cell* **129**,
551 1415-1426 (2007).
552 76 Zhu, Y., Aebersold, R., Mann, M. & Guo, T. SnapShot: Clinical proteomics. *Cell* **184**, 4840-
553 4840. e4841 (2021).
554

MATERIALS & METHODS

Plasmids

For expression and purification from bacteria, DNA sequences for the human Ser/Thr kinases, kinase binding partners, and chaperones listed below were codon-optimized for E. coli using GeneSmart prediction software (Genscript). Optimized coding sequences were synthesized as gBlocks (Integrated DNA Technologies) carrying 16-base pair overhangs at the 5' and 3' ends to facilitate in-fusion cloning (Clontech) into pET expression vectors (EMD MIllipore).

pCDFDuet1 constructs:

HSP90AA1-His_6 (full length), hereafter referred to as "HSP90," untagged HSP90 (full length), His_6-MO25a (full length), His_6-ALPHAK3/ALPK1 NTD (1-474), and His_8-CCNC (full length) in tandem with MED12-His_8 (1-100), and untagged CK2B (full length).

pET28a constructs:

His_6-PDPK1 (full length), His_6-PRP4/PRPF4B (519-end), GST-CHAK1/TRPM6 (1699-end), His_6-caMLCK/MYLK3 (490-end), untagged MEK5/MAP2K5-DD (full length), His_6-ERK7/MAPK15 (full length), His_6-SUMO-ALPHAK3/ALPK1 CTD (959-end), MYO3A-His_6 (1-308), His_6-NIK/MAP3K14 (327-673), and BMPR2-His_6 (172-504).

pETDuet1 constructs:

His_6-CDK8 (full length), His_6-CDK19 (full length), ERK5/MAPK7-His_6 (1-405), His_6-AAK1 (27-365), His_6-BIKE (37-345), CK2A1-His_6 (full length), CK2A2-His_6 (full length), His_{10}-MBP-MEKK1/MAP3K1 (1174-end), His_6-CLK1 (128-end), His_8-PLK2 (57-360), His_{10}-MAP3K15 (631-922), His_6-SUMO-ASK1/MAP3K5 (659-951), and His_6-TAO2 (1-350).

pACYDuet1 construct:

Untagged CDC37 (full length).

Mammalian expression constructs

For enhanced expression in mammalian lines cells, the DNA sequences of His_6-GST-SBK (full length) and Flag-His_6-WNK3 (1-434) were optimized for expression in H. sapiens using GeneSmart (Genscript) and synthesized as gBlocks (Integrated DNA Technologies) carrying 16-base pair overhangs to facilitate in-fusion cloning into digested pCDNA3.4 (Thermo).

To generate a mammalian expression construct for the TAK1/MAP3K7, the coding sequence for this kinase (GE Healthcare Dharmacon: MHS6278-202756930) and its binding partner TAB1 (GE Healthcare Dharmacon: MHS6278-202760135) were PCR amplified and ligated as a fusion construct (TAK1 (1-303)-TAB1(451-end)) into the mammalian expression vector pLenti-X by in-fusion.

Expression constructs purchased or obtained from other laboratories:

Bacterial expression constructs for GST-VRK1 (full length) and GST-VRK2 (full length), in pGEX-4T, were received as gifts from Pedro Lazo at CSIC-Universidad de Salamanca [1]. Bacterial expression construct for mouse CDKL5-His_6 (1-352), in pET23a+, was received as a gift from Syouichi Katayama at Ritsumeikan University [2]. Bacterial expression constructs for His_6-SUMO-PDHK1 (full length), His_6-SUMO-PDHK4 (full length), pGroESL (GroEL/GroES), and MBP-BCKDK (full length) were received as gifts from David Chuang, Shih-Chia Tso, and Richard Wynn at UT Southwestern Medical Center [3,4]. pProEx HTa-BRAF_16mut V600E (444-721) was a gift from Marc Therrien at Université de Montréal [5]. Mammalian expression constructs for Flag-ATR (S1333A) and HA-ATRIP were provided by David Cortez at Vanderbilt University School of Medicine [6]. Bacterial expression constructs for DMPK1, CAMK1A, CAMK1G, CAMK2G, PHKG2, CDKL1, GAK, and lambda phosphatase were purchased from Addgene (Addgene Kit #1000000094) [7].

Expression and Purification from bacteria

Transformations were performed with BL21 Star cells (Thermo Fisher) unless specified otherwise. Antibiotic concentrations used: Carbenicillin (100 mg/L), Kanamycin (50 mg/L), Spectinomycin (25 mg/L), and Chloramphenicol (25 mg/L in EtOH, prepared fresh). Transformed cells were

grown in 1L Terrific broth by shaking at 190 rpm at 37°C until optical density reached 0.7-0.8, at which point 1mM IPTG was added to induce expression. The cells were then transferred to a refrigerated shaker and shaken at 220 rpm at 18°C for 16-20 hours. Cells were centrifuged at 6,000 x g, and pellets were snap freezed in liquid nitrogen and stored at -80 °C.

All steps in the protein purification were performed at 4°C. Cell pellet was solubilized in lysis buffer (see contents below), using spatula to disperse, and lysed by probe sonication. The lysate was centrifuged at 20,000 x g for 1 h and the supernatant was combined with affinity purification resin, nickel NTA (Qiagen) or glutathione sepharose (GE Health), that had been rinsed in base buffer. The supernatant-bead slurry was agitated using a rotisserie for 30 minutes. Resin was washed with 1 L base buffer and eluted in 10 bed volumes of elution buffer. Eluted protein was concentrated using Ultra Centrifugal Filter Units (Amicon), supplemented with 1 mM DTT and 25% glycerol, and snap freezed in liquid nitrogen and stored at -80 °C.

Standard lysis buffer: 50 mM Tris pH 8.0, 100 mM NaCl, 2 mM MgCl2, 2% glycerol, HALT EDTA-free phosphatase and protease inhibitor cocktail (Life technologies), 5 mM beta-mercaptoethanol, 1-3 grams of lysozyme (Sigma)
Standard base buffer: 50 mM Tris pH 8.0, 100 mM NaCl, 2 mM MgCl2, 2% glycerol
(include 50 mM imidazole for purifications involving polyhistidine-tag)
Standard wash buffer: 50 mM Tris pH 8.0, 500 mM NaCl, 2 mM MgCl2, 2% glycerol (include 50 mM imidazole for purifications involving polyhistidine-tag)
Polyhistidine-tag elution buffer: 50 mM Tris pH 8.0, 100 mM NaCl, 2 mM MgCl2, 2% glycerol, 350 mM imidazole
GST-tag elution buffer: 50 mM Tris pH 8.0, 100 mM NaCl, 2 mM MgCl2, 2% glycerol, 10 mM glutathione (pH adjusted after addition of glutathione)

The kinases BRAF and NIK were co-expressed with untagged HSP90/CDC37. CDK8 was co-purified with CCNC/MED12. CDK19 was co-purified with CCNC/MED12 pCDFDuet1. CK2A1 and CK2A2 were co-purified with CK2B. ERK5 was co-expressed with MEK5DD. ALPHAK3 NTD (pCDFDuet1) and CTD (pETDuet1) were co-purified. DMPK1, CAMK1A, CAMK1G,

CAMK2G, PHKG2, CDKL1, and GAK were co-expressed with lambda phosphatase in Rosetta 2 cells (Novagen).

PDHK1, PDHK4, BCKDK were co-expressed with GroeL/GroeS and purified with the following buffers: Lysis buffer (100 mM potassium phosphate pH 7.5, 10 mM L-arginine (stock pH-adjusted to 7.5), 500 mM KCl, 0.1 mM EDTA, 0.1 mM EGTA, 0.2% Triton X-100, lysozyme), wash buffer (50 mM potassium phosphate pH 7.5, 10 mM arginine, 500 mM NaCl, 0.1% Triton X-100, 2 mM MgCl2), and Elution buffer (25 mM Tris pH 7.5, 120 mM KCl, 0.02% Tween-20, 50 mM Arginine, 350 mM imidazole for PDHK1 and PDHK4 only, 20 mM maltose for BCKDK only). BCKDK was purified by its MBP tag on amylose resin (NEB).

CDKL5 was expressed in BL21-codonplus(DE3)-RIL cells.

KIS (full length) was purified as described previously[8].

Expression and purification from mammalian cells

Transfection

Expi293F cells (Thermo Fisher) were cultured in 500mL Expi293 Expression Medium (Thermo Fisher) in 2L spinner flasks on a magnetic stirring platform at 100 RPM at 36.8°C with 8% CO_2. For transfection, 500 µg of expression constructs were diluted in Opti-MEM I Reduced Serum Medium (Thermo Fisher). ExpiFectamine 293 Reagent (Thermo Fisher) was diluted with Opti-MEM separately then combined with diluted plasmid DNA for 10 minutes at room temperature. The mixture was then transferred to the cells (3 X 10^6 cells/mL) and stirred. 20 hours after transfection, ExpiFectamine 293 Transfection Enhancer 1 and Enhancer 2 (Thermo Fisher) were added to the cells. Two days later, the cells were centrifuged at 300 X g for 5 min, snap freezed in liquid nitrogen, and stored at -80°C (3 days post-transfection).

Purification

All steps of protein purification were performed at 4°C. Cell pellet was solubilized in lysis buffer, using spatula to disperse, and lysed by Dounce homogenization (20 strokes). The lysate was centrifuged at 100,000 x g for 1 h and the supernatant was combined with affinity purification resin, nickel NTA (Qiagen), glutathione sepharose (GE Health), or Anti-Flag M2 affinity gel

(Sigma), and agitated on rotisserie for 30 min (nickel and glutathione beads) or 1 hour (Anti-flag beads). Resin was washed with 1 L base buffer and eluted in 10 bed volumes of elution buffer. For elution of flag tagged-proteins, beads were immersed in elution buffer (0.15 ug/mL 3X Flag peptide (Sigma)) and agitated on rotisserie for 1 hour prior to elution. Eluted protein was concentrated using Ultra Centrifugal Filter Units (Amicon), supplemented with 1 mM DTT and 25% glycerol, and snap freezed in liquid nitrogen and stored at -80°C.

Standard lysis buffer: 50 mM Tris pH 8.0, 150 mM NaCl, 2 mM $MgCl_2$, 5% glycerol, 1% Triton X-100, 5 mM β-mercaptoethanol, HALT protease inhibitors.
Standard base buffer: 50 mM Tris pH 8.0, 100 mM NaCl, 2 mM $MgCl_2$, 2% glycerol.
Standard wash buffer: 50 mM Tris pH 8.0, 500 mM NaCl, 2 mM $MgCl_2$, 2% glycerol.

His_6-GST-tagged SBK was purified sequentially on nickel and then glutathione resins. The first wash buffer included 25 mM imidazole. SBK1 elution buffer for polyhistidine tag: 50 mM Tris pH 8.0, 100 mM NaCl, 2 mM $MgCl_2$, 2% glycerol, 250 mM imidazole. SBK1 elution buffer for GST tag: 50 mM Tris pH 8.0, 100 mM NaCl, 2 mM $MgCl_2$, 2% glycerol, 10 mM glutathione.

Flag-TAK1-TAB1 elution buffer: 50 mM Tris pH 8.0, 100 mM NaCl, 2 mM $MgCl_2$, 2% glycerol, 0.15 ug/mL 3X Flag peptide.

Flag-His_6-WNK3 was purified sequentially on nickel and then anti-flag resins. The first wash buffer contained 25 mM imidazole. Flag-tag elution buffer (chloride-free): 50 mM Tris pH 7.5, 2 mM $MgAc_2$, 2% glycerol, 0.15 ug/mL 3X Flag peptide.

350 uL Flag-ATR (S1333A) and 150 ug Ha-ATRIP were co-transfected into Expi293 cells and incubated for one additional day following addition of enhancers (4 days post-transfection).
ATR lysis buffer: 50 mM HEPES pH 7.4, 150 mM NaCl, 10% glycerol, 0.25% Tween 20, 2 mM MgCl2, DTT.
ATR wash buffer: 50 mM HEPES pH 7.4, 150 mM NaCl, 0.01% Brij-35, 2 mM MgCl2, 5 mM ATP, DTT.

ATR elution buffer: 20 mM HEPES pH 7.4, 150 mM NaCl, 0.01% Brij-35, DTT, 0.15 ug/mL 3X Flag peptide.
Eluates were concentrated to 1 mL in 100K MWCO Amicon tubes and resolved by MonoS column in in 0-1M NaCl gradient (buffer 25 mM Bis Tris pH 6.9, 0.01% Brij-35, and 5 mM TCEP). 1 mL fraction were collected. Fractions 1-4 were combined and concentrated to 1 mL in 100K MWCO and resolved by size exclusion (Superose 6) in 20 mM HEPES pH 7.4, 200 mM NaCl, 0.01% Brij-35, and 5 mM TCEP. 1 mL fraction were collected. Fractions 11-14 were verified to be pure ATR:ATRIP complex on SDS-PAGE and profiled in PSPA.

SMG1:SMG9 complexes were purified from HEK293T cells as described previously[9].

RIPK1, RIPK2, and RIPK3 were purified from insect cells as described previously[10].

Recombinant active kinases obtained from other laboratories:
Recombinant active CDK12:CycK, CDK13:CycK, and CDK9:CycT complexes were provided as gifts from Matthias Geyer at University of Bonn[11,12].
Recombinant active DCAMKL1/DCLK1 and MELK were provided as gifts from Nathanael Gray and Kenneth Westover[13,14].
Recombinant active PRPK(full length):CGI121(full length) complex was provided as a gift from Leo Wan and Frank Sicheri at the Lunenfeld-Tanenbaum Research Institute[15].
Recombinant active HASPIN (452-798) was provided as a gift from Andrea Musacchio at the Institute of Molecular Physiology in Dortmund[16].
Recombinant active YSK1 was provided as a gift from Xuelian Luo at UT Southwestern Medical Center[17].

Catalog and lot numbers of purchased recombinant kinases are listed in Table S1.

Peptide library arrays
Recombinant kinase was distributed across 384-well plate, mixed with the peptide substrate library in solution phase (Anaspec #AS-62017-1 and #AS-62335), and incubated for 90 mins (Assay conditions for each kinase described in Table S1)[18-22]. Each well contains a mixture of peptides

with a centralized phosphor-acceptor (serine and threonine at a 1:1 ratio) and one fixed amino acid in a randomized background. All 20 natural amino acids, plus two PTM residues (phospho-Thr and phospho-Tyr), were substituted into positions -5 to +4 to generate 198 unique peptide mixtures (22 amino acids X 9 fixed positions). After reaction, peptides were separated were spotted on streptavidin-conjugated membranes (Promega #V2861) where they tightly associated via their C-terminal biotinylations. The membranes were rinsed to remove free ATP and kinase and imaged with Typhoon FLA 7000 phosphorimager (GE). Raw data (GEL file) was quantified by ImageQuant (GE). For the kinase ALPHAK3, spots were normalized to surrounding background, due to spatial variation in background signal. PDHK1 and PDHK4 showed dual specificity for serine and tyrosine. For these kinases, we utilized a customized peptide substrate library devoid of tyrosines at randomized positions.

In total, 286 human kinase motifs, one motif from a mouse kinase ortholog (CDKL5), and one motif from an arthropod Pediculus humanus corporis kinase ortholog (PINK1), were combined with 15 human kinase motifs we previously published, that included AKT1[23], SRPK1[24], SRPK2[24], SRPK3[24], CK1D[24], DYRK1A[25], DYRK2[25], GSK3A[25], GSK3B[25], CK1A[25], CK1E[25], CK1G1[25], CDK10[26], CDK2[27], CDK3[27], CDK18[27], and CDK7[28].

Matrix processing

The matrices were column-normalized (at all positions) by the sum of the 17 randomized amino acids (excluding serine, threonine, and cysteine), to yield positional specific scoring matrices (PSSMs). PDHK1 and PDHK4 were normalized by the 16 randomized amino acids (excluding serine, threonine, cysteine, and additionally tyrosine), corresponding to the uniquely customized peptide library that profiled these kinases. The cysteine row was scaled by its median to be 1/17 (1/16 for PDHK1 and PDHK4). The serine and threonine values in each position were set to be the median of that position. The ratio of serine vs threonine phospho-acceptor favorability (S_0 and T_0, respectively) was determined by summing up the values of the serine and threonine rows in the densitometry matrix (S_S and S_T, respectively), and then normalized by the higher value among the two:

$$S_S = \sum_{p=-5}^{+4} M_{S,p} \; ; \; S_T = \sum_{p=-5}^{+4} M_{T,p}$$

$$S_0 = \frac{S_s}{max(S_S, S_T)} \; ; \; T_0 = \frac{S_T}{max(S_S, S_T)}$$

Matrix clustering

The dendrogram in Fig. 2 was generated using the normalized matrices with the 20 unmodified amino acids, as well as phosphothreonine and phosphotyrosine. Linkage matrix was computed through the SciPy package in Python (v1.7.1), using 'ward' method. Results were converted to Newick tree format and plotted using FigTree (v1.4.4).

Substrate scoring

For scoring substrates, the values of the corresponding amino acids in the corresponding positions were multiplied and scaled by the probability of a random peptide:

$$Raw\ Score_{Kin\ X} = \frac{\prod_{Pos} P_{Kin\ X}(AA, Position)}{\left(\frac{1}{\#Random\ AA}\right)^{length(positions)}}$$

For the percentile-score of a substrate by a given kinase, we first computed the *a priori* score distribution of that kinase by scoring all the reported S/T phosphorylation sites on PhosphoSitePlus[29] (downloaded on July 2021) with at least five high-throughput detections or one low-throughout detection, by the method discussed earlier. The percentile-score of a kinase-substrate pair is defined as the percentile ranking of the substrate within the score distribution of each kinase. This value was used for kinase enrichment as described before.

Kinase enrichment analysis

The single phosphorylation sites (not including multi-phosphorylated peptides) in the analyzed phosphoproteomics studies were scored by all the characterized kinases (303 S/T kinases), and

their ranks in the known phosphoproteome score distribution were determined as described above. For every non-duplicate, singly phosphorylated site, kinases that ranked within the top-15 kinases for the S/T kinases were considered as biochemically favored kinases for that phosphorylation site. For assessing kinase motif enrichment in phosphoproteomics datasets, we compared the percentage of phosphorylation sites for which each kinase was predicted among the upregulated/downregulated (increased/decreased, respectively) phosphorylation sites (sites with |log2Fold-Change| equal or greater than the logFC threshold), versus the percentage of biochemically favored phosphorylation sites for that kinase within the set of unregulated (unchanged) sites in this study (sites with |log2Fold-Change| less than the logFC threshold). LogFC threshold was determined to be 1.5 for all panels in Fig. 4, except for Fig. 4e where the threshold was set to 0.5 due to low range of the logFC in the data. Contingency tables were corrected using Haldane correction (adding 0.5 to the cases with zero in one of the counts). Statistical significance was determined using one-sided Fisher's exact test, and the corresponding p-values were adjusted using the Benjamini-Hochberg procedure. Kinases that were significant (adjusted p-value <= 0.1) for both upregulated and downregulated analysis were excluded from downstream analysis. Then, for every kinase, the most significant enrichment side (upregulated or downregulated) was selected based on the adjusted p-value and presented in the volcano plots.

Sequence logos

Sequence logos were made using logomaker package in Python[30]. For individual kinases, the normalized matrix was used, where the height of every letter is the ratio of its value to the median value of that position. The serine and threonine heights in the central position (position zero) were set to the ratio between their favorability, and to sum up to the maximal height in the peripheral positions. For clustered groups of kinases, the average matrix was calculated and presented as sequence logo as described above.

Comparative analyses between amino acids in the kinase domains and their substrate specificities

For Fig. S7, kinases were sorted by their log2(S0/T0) values. For the sequence logo, kinase domains of 290 available kinases were obtained from previously aligned kinase sequences [PMID: 31875044]. The alignments to residues Met1-Leu296 in CDK2 (PDB: 1QMZ) were obtained for

each kinase, and the frequencies of amino acids for each 15 kinases were calculated and plotted as a sequence logo.

Known kinase-substrate pairs

Experimentally validated kinase-substrate relationships were obtained from PhosphoSitePlus (July 2021, Table S2). Number of reports for each pair was determined by the sum of the *in vivo* and *in vitro* reports.

Illustrations

Experimental schema and illustrative models were generated by BioRender (https://biorender.com/) and Chemdraw. Kinome images generated and modified using Coral: http://phanstiel-lab.med.unc.edu/CORAL/. Structural illustrations were generated with PYMOL. Generic kinase domains in Figs 1 and 3: PKAα (pdb 1ATP). Kinase and substrate structures in Fig. 3: ATM (pdb 7SIC), p53 (chimera of alphaFold AF-P04637-F1-model_v2_1 (1-95) and 2ATA (96-292)), PHKG2 (pdb 2Y7J), and PYGM (pdb 1ABB)

References

1 Sanz-García, M. *et al.* Substrate profiling of human vaccinia-related kinases identifies coilin, a Cajal body nuclear protein, as a phosphorylation target with neurological implications. *Journal of proteomics* **75**, 548-560 (2011).

2 Sekiguchi, M. *et al.* Identification of amphiphysin 1 as an endogenous substrate for CDKL5, a protein kinase associated with X-linked neurodevelopmental disorder. *Archives of biochemistry and biophysics* **535**, 257-267 (2013).

3 Wynn, R. M., Davie, J. R., Cox, R. P. & Chuang, D. T. Chaperonins groEL and groES promote assembly of heterotetramers (alpha 2 beta 2) of mammalian mitochondrial branched-chain alpha-keto acid decarboxylase in Escherichia coli. *Journal of Biological Chemistry* **267**, 12400-12403 (1992).

4 Song, J.-L., Li, J., Huang, Y.-S. & Chuang, D. T. Encapsulation of an 86-kDa assembly intermediate inside the cavities of GroEL and its single-ring variant SR1 by GroES. *Journal of Biological Chemistry* **278**, 2515-2521 (2003).

5 Thevakumaran, N. *et al.* Crystal structure of a BRAF kinase domain monomer explains basis for allosteric regulation. *Nature structural & molecular biology* **22**, 37-43 (2015).

6 Luzwick, J. W., Nam, E. A., Zhao, R. & Cortez, D. Mutation of serine 1333 in the ATR HEAT repeats creates a hyperactive kinase. *PLoS One* **9**, e99397 (2014).

7 Albanese, S. K. *et al.* An open library of human kinase domain constructs for automated bacterial expression. *Biochemistry* **57**, 4675-4689 (2018).
8 Manceau, V. *et al.* Major phosphorylation of SF1 on adjacent Ser-Pro motifs enhances interaction with U2AF65. *The FEBS journal* **273**, 577-587 (2006).
9 Melero, R. *et al.* Structures of SMG1-UPFs complexes: SMG1 contributes to regulate UPF2-dependent activation of UPF1 in NMD. *Structure* **22**, 1105-1119 (2014).
10 Najjar, M. *et al.* Structure guided design of potent and selective ponatinib-based hybrid inhibitors for RIPK1. *Cell reports* **10**, 1850-1860 (2015).
11 Czudnochowski, N., Bösken, C. A. & Geyer, M. Serine-7 but not serine-5 phosphorylation primes RNA polymerase II CTD for P-TEFb recognition. *Nature communications* **3**, 1-12 (2012).
12 Greifenberg, A. K. *et al.* Structural and functional analysis of the Cdk13/Cyclin K complex. *Cell reports* **14**, 320-331 (2016).
13 Liu, Y. *et al.* Chemical biology toolkit for DCLK1 reveals connection to RNA processing. *Cell chemical biology* **27**, 1229-1240. e1224 (2020).
14 Ferguson, F. M. *et al.* Discovery of a selective inhibitor of doublecortin like kinase 1. *Nature chemical biology* **16**, 635-643 (2020).
15 Beenstock, J. *et al.* A substrate binding model for the KEOPS tRNA modifying complex. *Nature communications* **11**, 1-17 (2020).
16 Villa, F. *et al.* Crystal structure of the catalytic domain of Haspin, an atypical kinase implicated in chromatin organization. *Proceedings of the National Academy of Sciences* **106**, 20204-20209 (2009).
17 Bae, S. J., Ni, L. & Luo, X. STK25 suppresses Hippo signaling by regulating SAV1-STRIPAK antagonism. *Elife* **9**, e54863 (2020).
18 Murillo-de-Ozores, A. R., Chávez-Canales, M., de Los Heros, P., Gamba, G. & Castañeda-Bueno, M. Physiological processes modulated by the chloride-sensitive WNK-SPAK/OSR1 kinase signaling pathway and the cation-coupled chloride cotransporters. *Frontiers in Physiology*, 1353 (2020).
19 Filippi, B. M. *et al.* MO25 is a master regulator of SPAK/OSR1 and MST3/MST4/YSK1 protein kinases. *The EMBO journal* **30**, 1730-1741 (2011).
20 Zhou, P. *et al.* Alpha-kinase 1 is a cytosolic innate immune receptor for bacterial ADP-heptose. *Nature* **561**, 122-126 (2018).
21 Taipale, M. *et al.* Quantitative analysis of HSP90-client interactions reveals principles of substrate recognition. *Cell* **150**, 987-1001 (2012).
22 Klatt, F. *et al.* A precisely positioned MED12 activation helix stimulates CDK8 kinase activity. *Proceedings of the National Academy of Sciences* **117**, 2894-2905 (2020).
23 Balasuriya, N. *et al.* Phosphorylation-dependent substrate selectivity of protein kinase B (AKT1). *Journal of Biological Chemistry* **295**, 8120-8134 (2020).
24 Yaron, T. M. *et al.* The FDA-approved drug Alectinib compromises SARS-CoV-2 nucleocapsid phosphorylation and inhibits viral infection in vitro. *BioRxiv* (2020).
25 Zheng, Y. *et al.* Regulation of folate and methionine metabolism by multisite phosphorylation of human methylenetetrahydrofolate reductase. *Scientific reports* **9**, 1-11 (2019).

26 Robert, T. *et al.* Development of a CDK10/CycM in vitro kinase screening assay and identification of first small-molecule inhibitors. *Frontiers in chemistry* **8**, 147 (2020).
27 Ferguson, F. M. *et al.* Discovery of covalent CDK14 inhibitors with pan-TAIRE family specificity. *Cell chemical biology* **26**, 804-817. e812 (2019).
28 Rimel, J. K. *et al.* Selective inhibition of CDK7 reveals high-confidence targets and new models for TFIIH function in transcription. *Genes & development* **34**, 1452-1473 (2020).
29 Hornbeck, P. V. *et al.* 15 years of PhosphoSitePlus®: integrating post-translationally modified sites, disease variants and isoforms. *Nucleic Acids Research* **47**, D433-D441 (2019).
30 Wagih, O. ggseqlogo: a versatile R package for drawing sequence logos. *Bioinformatics* **33**, 3645-3647 (2017).

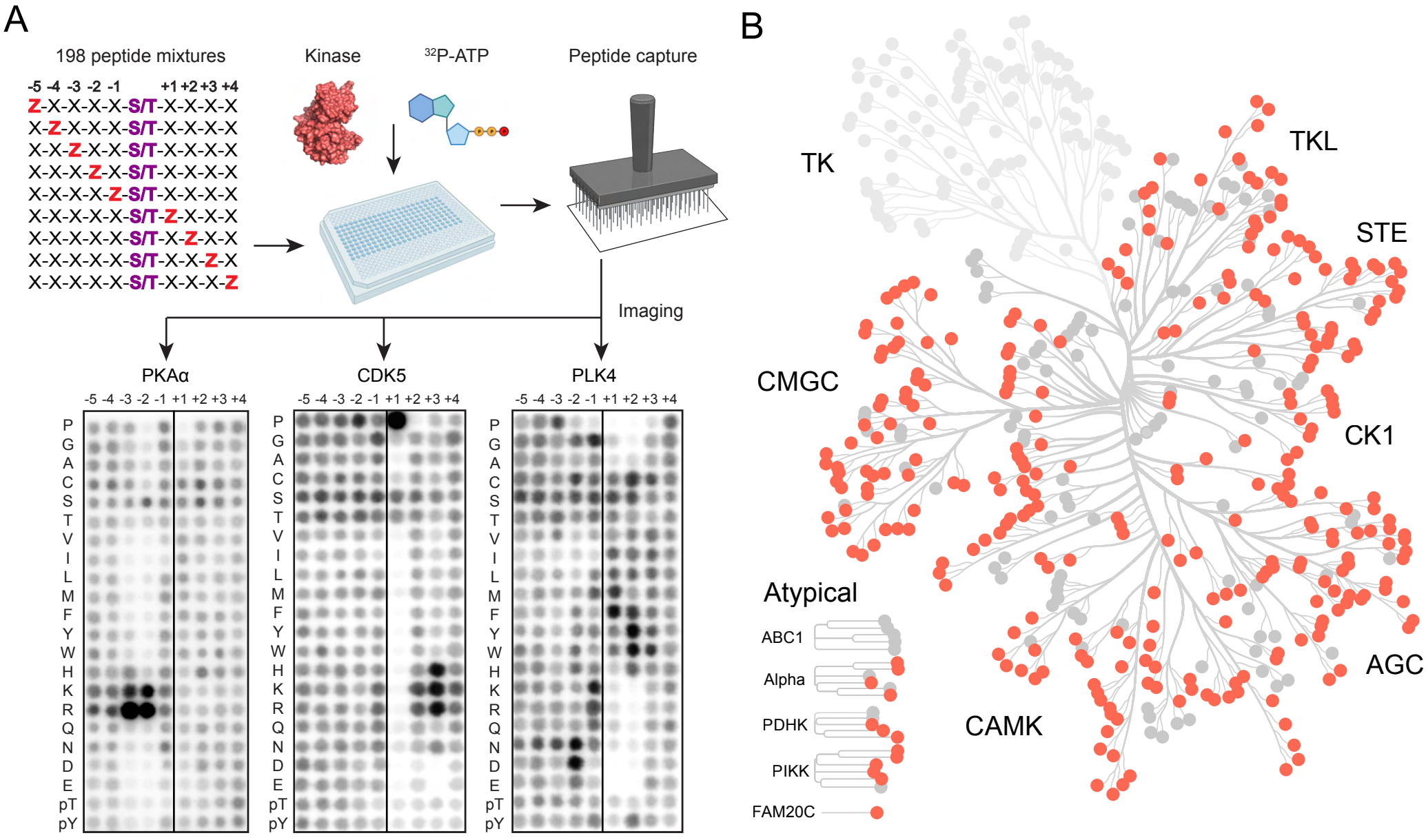

Fig. 1 Profiling the substrate specificity of the human serine/threonine kinome.
(A) Experimental workflow for positional scanning peptide arrays and representative results. (B) Dendrogram of the human protein kinome that highlights the serine/threonine kinases analyzed in this work.

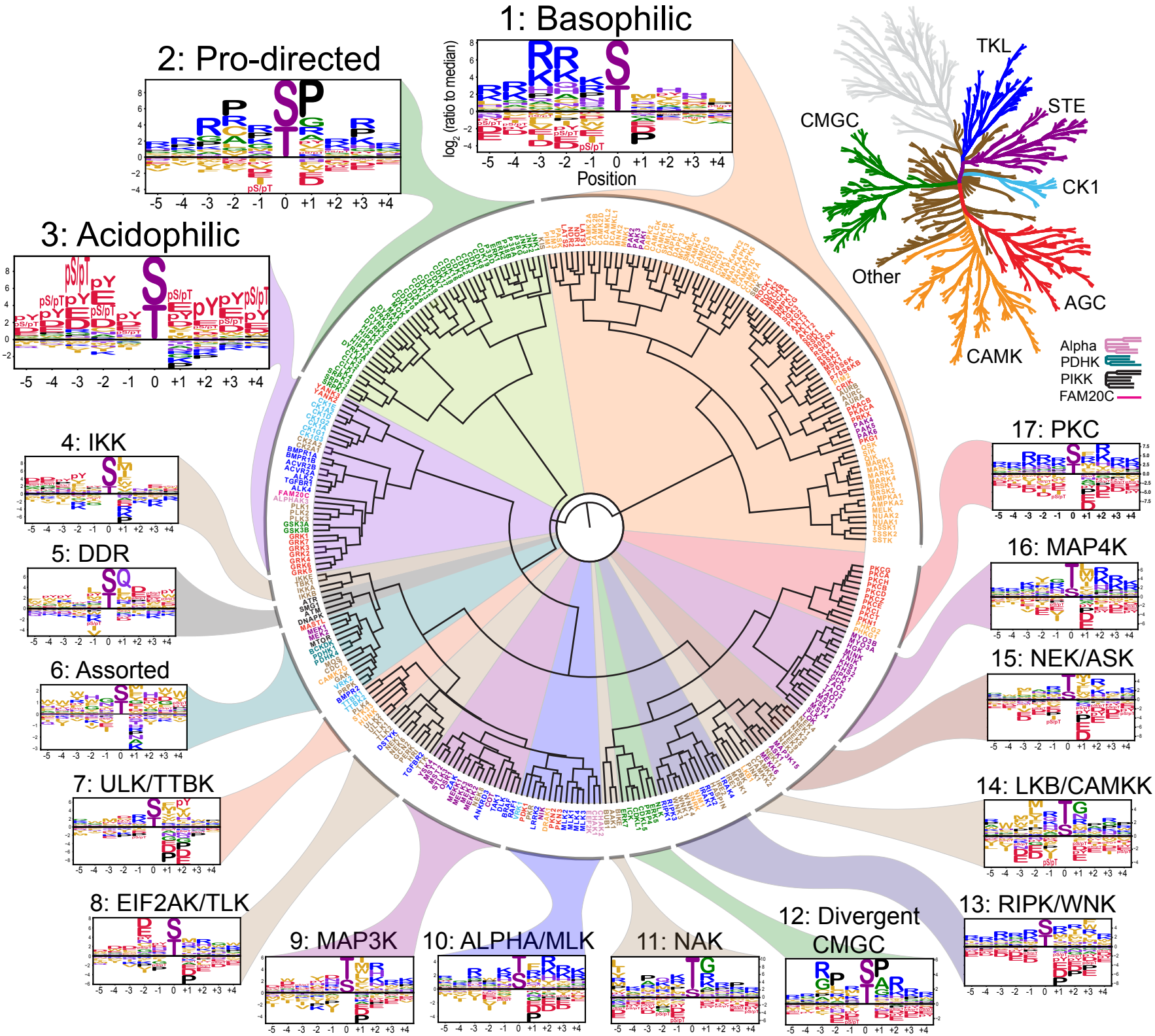

Fig. 2 Phosphorylation site motif tree of the human Ser/Thr kinome.
Hierarchichal clustering of 303 Ser/Thr kinase position specific scoring matrices (PSSMs). Kinase names are color-labeled according to their phylogenetic relationships (top right)[2].

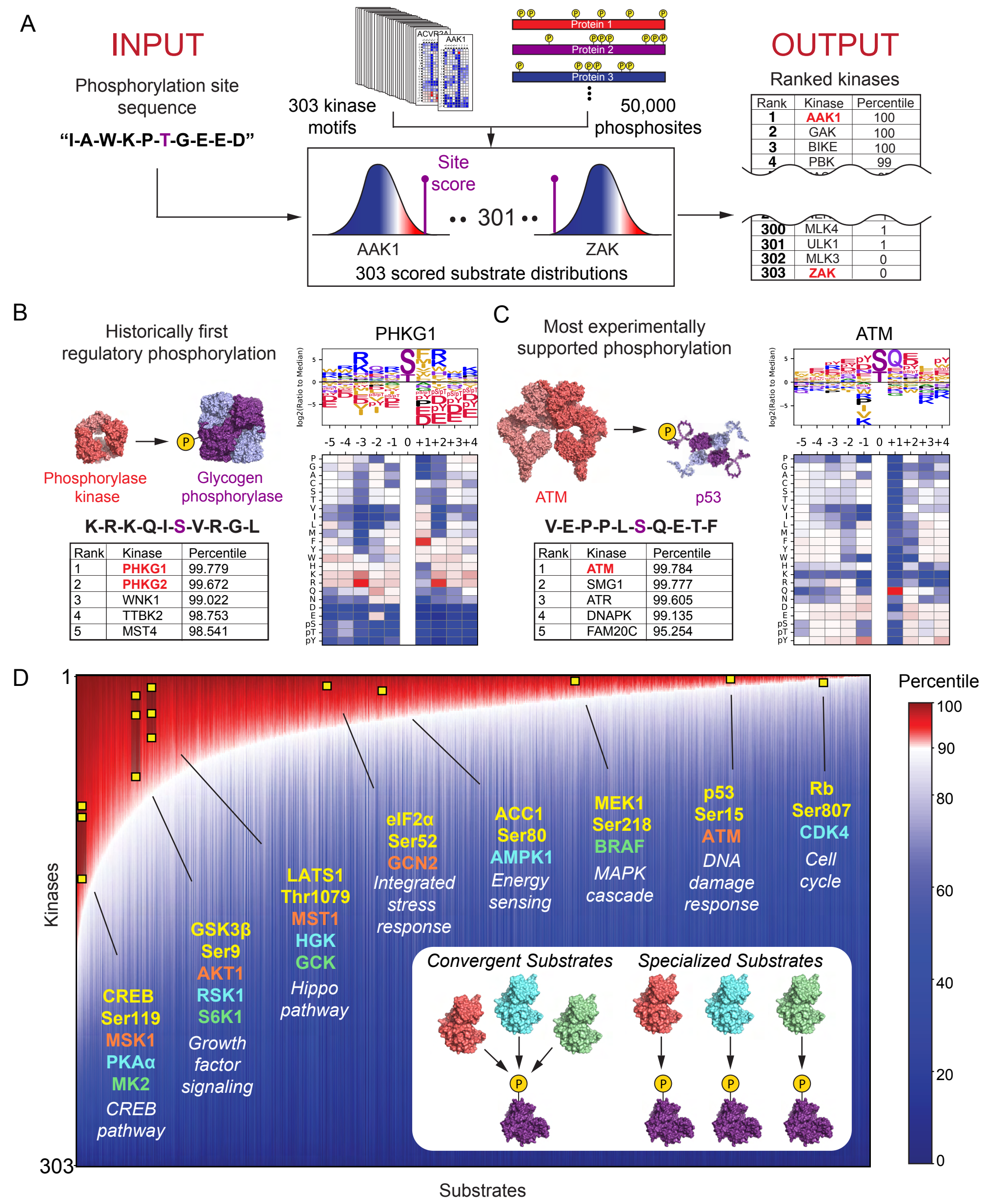

Fig. 3 Phosphorylation motifs for the human serine/threonine kinome allow comprehensive scoring and annotation of the human phosphoproteome.
(A) Schematic of the substrate scoring process. (B) Results for Ser15 on glycogen phosphorylase alongside PSSM and substrate motif logo of its established kinase glycogen phosphorylase kinase. (C) Results for Ser15 on p53 alongside its established kinase ATM. (D) Annotation of the human Ser and Thr phosphoproteome by percentile-scores from 303 Ser/Thr kinases as illustrated in (A). ~50,000 scored phosphorylation sites were sorted along the x-axis by their median kinase percentile-score. On the y-axis, kinase percentile scores were sorted by rank separately for each site and represented by heatmap. Examples of well-studied kinase-substrate relationships are highlighted (yellow squares). Inset: Phosphorylation sites on the left end of plot scored favorably for many kinases while sites on the right end scored favorably for fewer kinases.

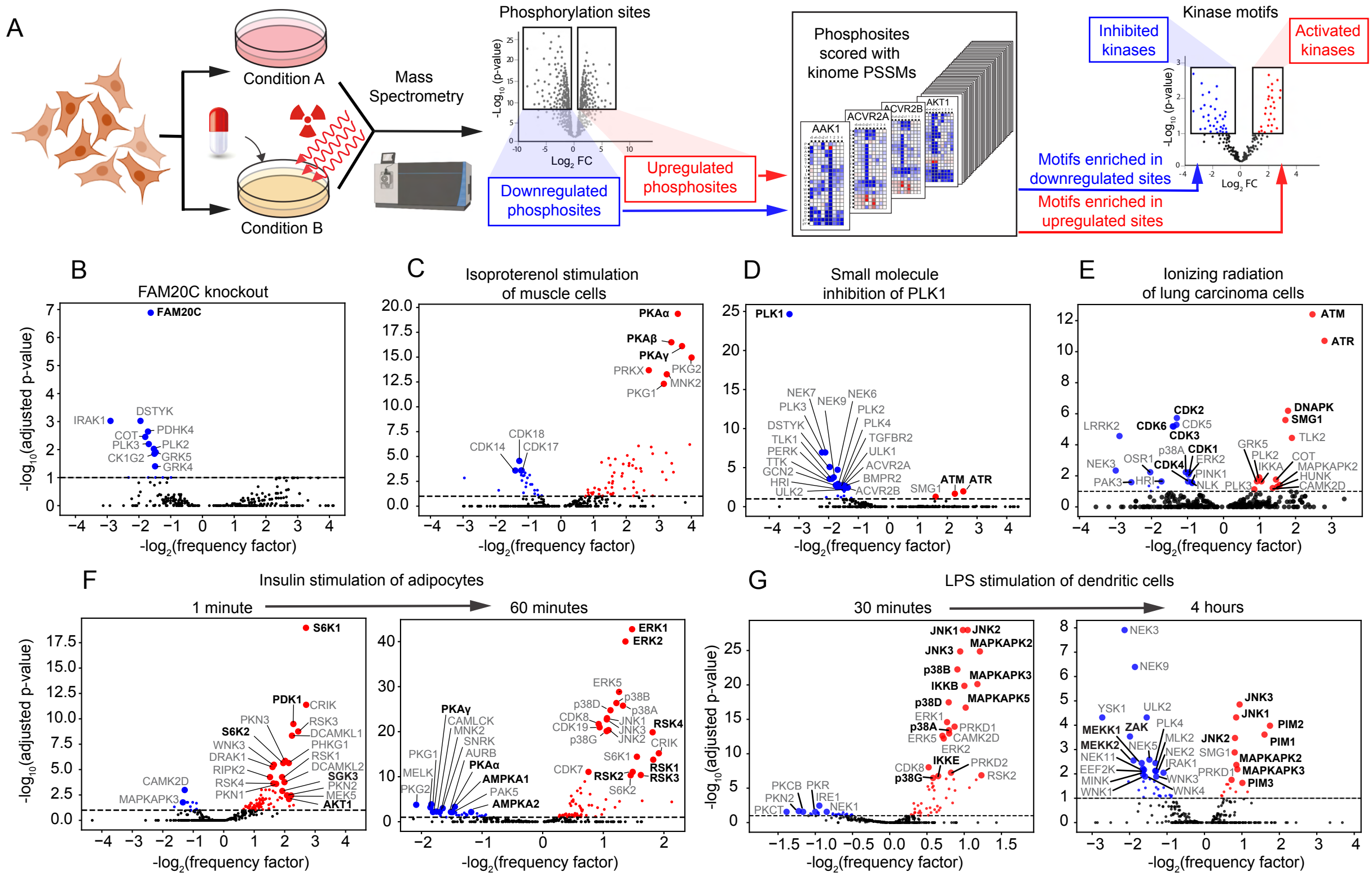

Fig. 4 Global motif analysis reveals how kinase perturbations and pathway rewiring reshape the phosphoproteome.
(A) Schematic depiction of motif enrichment analysis of phosphoproteomics data. (B-G) Results from published datasets: (B) conditioned medium of HepG2 cells following genetic deletion of FAM20C[58], (C) cultured myotubes following 30-minute treatment with 2 μM isoproterenol[59], (D) HeLa cells following mitotic arrest by 45-minute treatment with 0.1 μM PLK1 inhibitor BI-2536[62], (E) A549 cells 2 hours following exposure to 6 Gy of ionizing radiation[65], (F) 3T3-L1 adipocytes following serum starvation and then 1-minute and 60-minute treatment with 100 nM insulin[70], (G) C57BL/6J mouse bone-marrow derived dendritic cells following 30-minute and 4-hour treatment with 100 ng/mL LPS[71].